Supplementary Material (ESI) for Chemical Communications
This journal is © The Royal Society of Chemistry 2013

Experimental details

The nickel phosphide thin films were electrochemically deposited on FTO glass (3.1 mm thick, 13 Ω/□, Nippon Sheet Glass) using potentiostatic (PS) and periodic pulse-reverse (PR) techniques at room temperature in a homemade three-electrode cell. FTO, Pt foil, and SCE (saturated calomel electrode) were used as the working, auxiliary, and reference electrodes, respectively. The deposition bath consisted of $NiSO_4 \cdot 6H_2O$ (80 g L^{-1}), $NiCl_2 \cdot 6H_2O$ (30 g L^{-1}), H_3PO_3 (25 g L^{-1}), and H_3PO_4 (40 g L^{-1}).[1] The PS deposition was carried out by applying a voltage of -0.8 V vs. SCE for 50 min. The periodic PR deposition was carried out by applying a voltage of -0.8 V vs. SCE for 6 s and a reverse voltage of 0.1 V vs. SCE for 24 s, the periodic voltage was repeated for 500 cycles.[2] After deposition, the film electrodes were rinsed with deionized water followed by heat-treated in nitrogen atmosphere at 500°C for 1 h. For comparison, the Pt/FTO electrode was fabricated by thermal decomposition of hexachloroplatinic acid (5 mM in isopropanol) on FTO glass at 425°C in air for 30 min.

The surface morphology and cross-sectional image of nickel phosphide film electrodes were examined with a field-emission electron microscope (FE-SEM, Jeol JEOL-6330). The X-ray diffraction (XRD) patterns of the nickel phosphide films were recorded by a diffractometer with a Cu Kα radiation source (wavelength = 1.54056 Å). The optical transmittance of the film electrodes was measured with an ultraviolet-visible spectrometer (UV-Vis, PerkinElmer Lambda 35) in the wavelength range of 300-800 nm. The cyclic voltammetry was carried out using a Pt foil as auxiliary electrode, Pt wire as reference electrode, and nickel phosphide electrode as working electrode with a total exposure area of 1.5×1.5 cm^2 in an acetonitrile solution containing 0.5 M $LiClO_4$, 50 mM LiI and 10 mM I_2. The scan rate is 10 mV s^{-1} and the electrochemical data were acquired using a potentiostat/galvanostat instrument (CH Instruments, CHI 608) coupled to a personal computer.

Nanostructured TiO_2 photoanodes were prepared by screen printing the TiO_2 slurry onto FTO glass and calcined at 450ºC for 1 h in air.[3] The thickness of resultant TiO_2 films was approximately 15 μm measured by the profiler. The adsorption of dye on the

TiO_2 surface was achieved by soaking the TiO_2 photoanodes in a dry ethanol solution containing N719 dye for 12 h at room temperature. A dye-adsorbed photoanode was assembled with a counter electrode by using a sealing plastic (Surlyn film, about 50 μm thick) to form a sandwich-type DSC. An electrolyte containing 0.6 M 1-propyl-2,3-dimethylimidazolium iodide, 0.1 M lithium iodide, 0.05 M iodine, and 0.5 M 4-tert-butylpyridine in acetonitrile solvent was then infiltrated into the space between the two electrodes of the DSC. The photocurrent-voltage characteristics under one-sun illumination (Yamashita Denso, YSS-E40; AM1.5, 100 mW cm^{-2}) were measured by scanning DSCs from the open-circuit voltage to the short-circuit condition at a scan rate of 5 mV s^{-1} with a source meter (Keithley, 2400). The electrochemical impedance spectroscopy (EIS) was carried out at open-circuit conditions using a potentiostat/galvanostat (CH Instruments, CHI 608) with ac amplitude of 10 mV at a frequency range of $0.05–1\times10^5$ Hz. For EIS measurements, a sandwich-type cell consisting of two nickel phosphide-coated FTO electrodes was used. The cell was filled with the same electrolyte as DSC. All chemicals used were of analytical grade and were used as received without further purification.

Electrochemical deposition

Fig. S1 shows the cyclic voltammogram (CV) of FTO electrode at a scan rate of 1 mV s^{-1} in the deposition bath. In the cathodic sweep, the electrodeposition of nickel phosphide takes place at voltages more negative than -0.6 V vs. SCE. The cathodic electrodeposition of nickel phosphide is generally accompanied with hydrogen evolution reaction, especially at more negative voltages. The adsorbed hydrogen may occupy the surface of the deposit and prevent the growth of regular layer and hence crystallization. There are two anodic peaks appear in the anodic sweep, which do not correspond to the dissolution of an alloy in two consecutive steps, but rather to that of two nickel phosphide alloys with different compositions, formed by two different kinetic processes.[4] The nickel phosphide alloy formed by potentiostatic electrodeposition may have Ni-rich regions in the bulk alloy.[4] Peaks A and B indicate the dissolutions of the Ni-rich region and the remainder of the nickel phosphide, respectively.[4] In the pulse-reverse electrodeposition, the anodic voltage was set at 0.1 V. Therefore, the Ni-rich regions may be dissolved. Periodically applying an anodic voltage following the cathodic deposition can remove the Ni-rich regions, leading to the

formation of porous nickel phosphide deposit with higher phosphorus content.

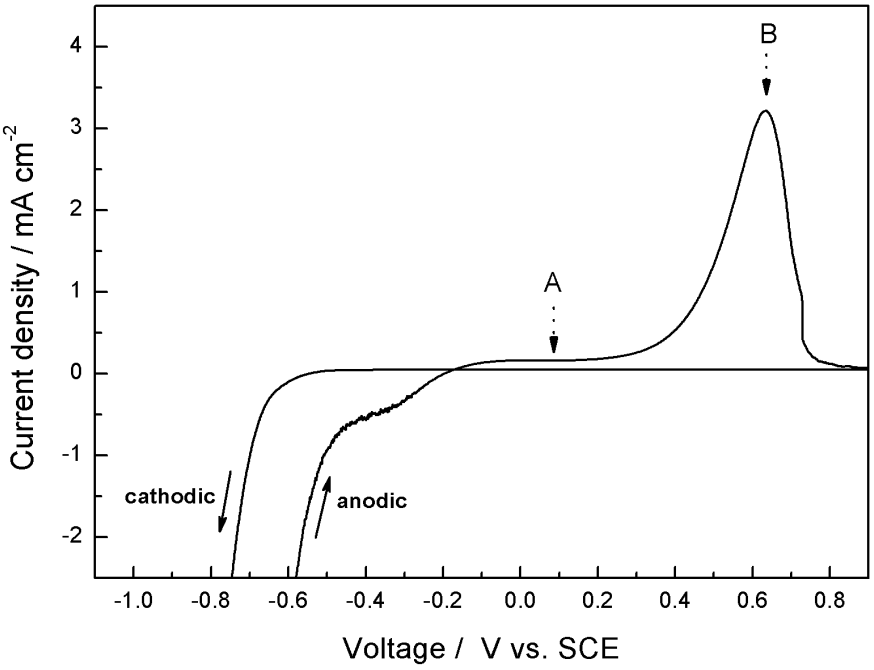

Fig. S1 CV curve of FTO electrode at a scan rate of 1 mV s^{-1} in the deposition bath.

In this work, the nickel phosphide films were prepared by both PS and PR methods using the same deposition bath. The cathodic deposition voltage was selected at -0.8 V vs. SCE for both methods to provide a certain overvoltage for deposition of nickel phosphide without a significant hydrogen evolution. The reverse voltage for PR deposition was set at 0.1 V to dissolve the Ni-rich regions in the bulk nickel phosphide alloy. Fig. S2 shows the current variations with time in different deposition methods. In the PS deposition, the current undergoes a rapid drop followed by a continuous increase. The voltage drop at the beginning of the deposition process is attributed to the depletion of nickel ions at the FTO surface.[2] A gradual increase in the current density results from the continuous growth of nickel phosphide deposits. In the PR deposition, an initial high current density appears at each reverse stage. In addition to electrical double-layer charging/discharging at the electrolyte/electrode interface, the high cathodic current density is attributed to a sufficiency of nickel ions at the electrode surface due to the anodic dissolution of freshly deposited Ni-rich regions. An initial high current density at each reverse stage is an evidence for the anodic dissolution of Ni-rich regions. The current density gradually decreases to zero at the end of each anodic process, indicating that most of the Ni-rich regions in the alloy have been dissolved, leaving a porous

nickel phosphide layer on the FTO surface.

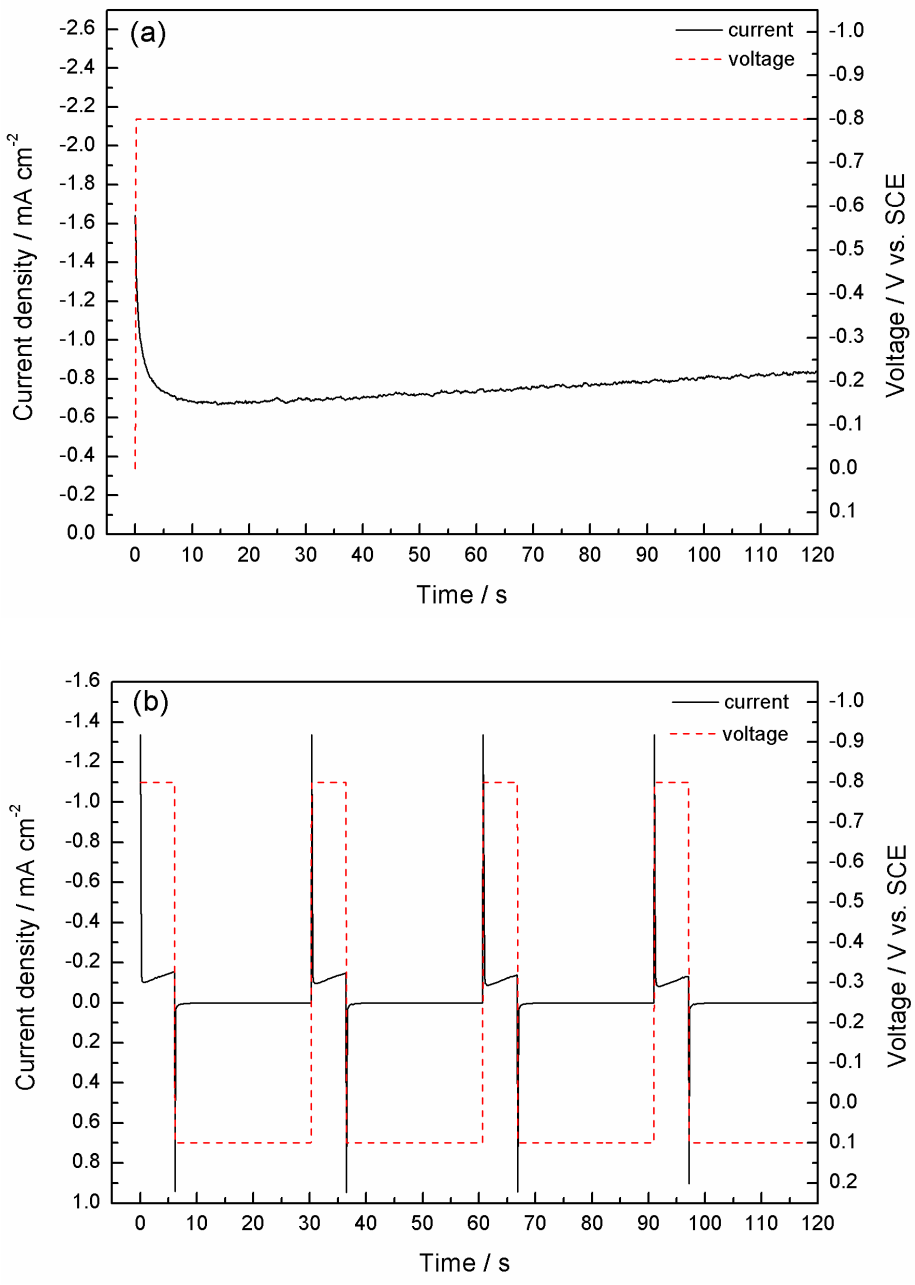

Fig. S2 Current variations with time in (a) PS deposition and (b) PR deposition.

X-ray diffraction patterns and UV-vis spectra

The chemical composition of nickel phosphide films were determined by XRD. To avoid the interference from FTO substrate, the nickel phosphide films were deposited on the carbon fabric instead of FTO substrate. Fig. S3 shows the XRD patterns of carbon fabric and nickel phosphide-coated carbon fabric. In addition to the characterization peaks of carbon fabric, the XRD pattern of nickel phosphide film

deposited by PS method resembles the $Ni_{12}P_5$ (JCPDS no. 74-1381), while that of nickel phosphide film deposited by PR method corresponds to the Ni_2P (JCPDS no. 74-1385). Clearly, the nickel phosphide deposited by PR method has phosphorus content slightly higher than that deposited by PS method. Anodic dissolution of Ni-rich regions is responsible for the higher phosphorus content in nickel phosphide deposit obtained by PR deposition. Ni_2P can also be prepared by PS method at -0.7 V vs. SCE.

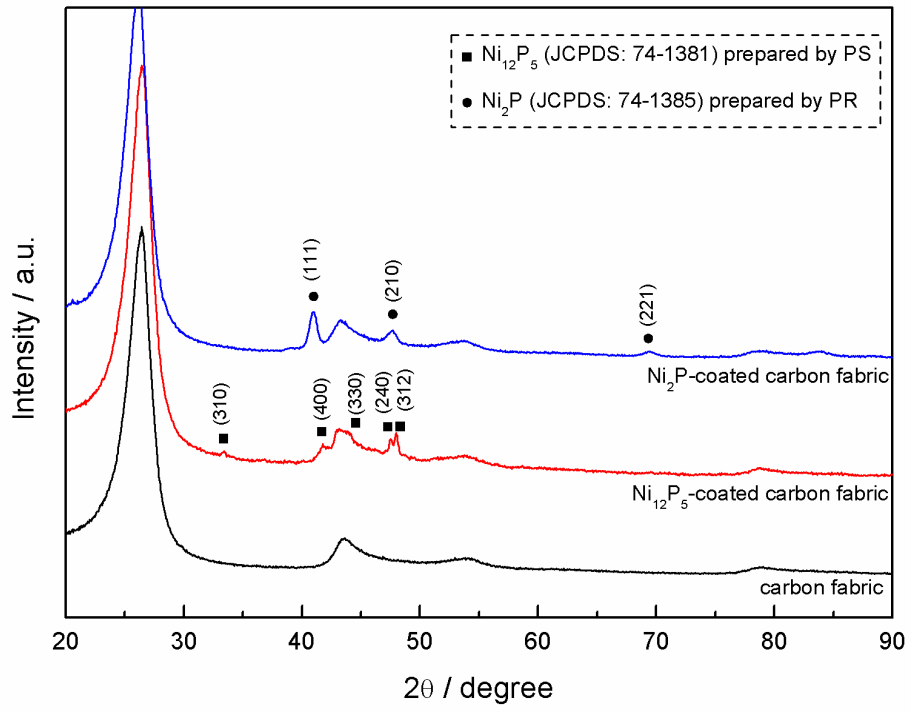

Fig. S3 XRD patterns of carbon fabric and nickel phosphide-coated carbon fabric.

Fig. S4 shows the UV-Vis absorption spectra of bare FTO, Pt-coated FTO, and nickel phosphide-coated FTO glass electrodes. All electrodes were annealed before measurements. The transmittance of FTO glass electrode is reduced after coated with Pt or nickel phosphide films. It is surprising to find that the Ni_2P-coated FTO prepared by PR method has a mean transmittance as high as 73.7% in the visible light region (wavelength range of 300-800 nm), which is only slightly lower than that of the bare FTO electrode (80.6%). The ultrathin film and porous nanosphere structure account for the high transmittance of Ni_2P electrode prepared by PR deposition. The mean transmittance of $Ni_{12}P_5$-coated FTO electrode prepared by PS method significantly decreases to 60.9%, probably due to the large particle size and compact structure of nanoparticles. Therefore, PR deposition features easy fabrication of transparent

nanolayer with well dispersed porous Ni_2P nanospheres on the FTO surface at room temperature.

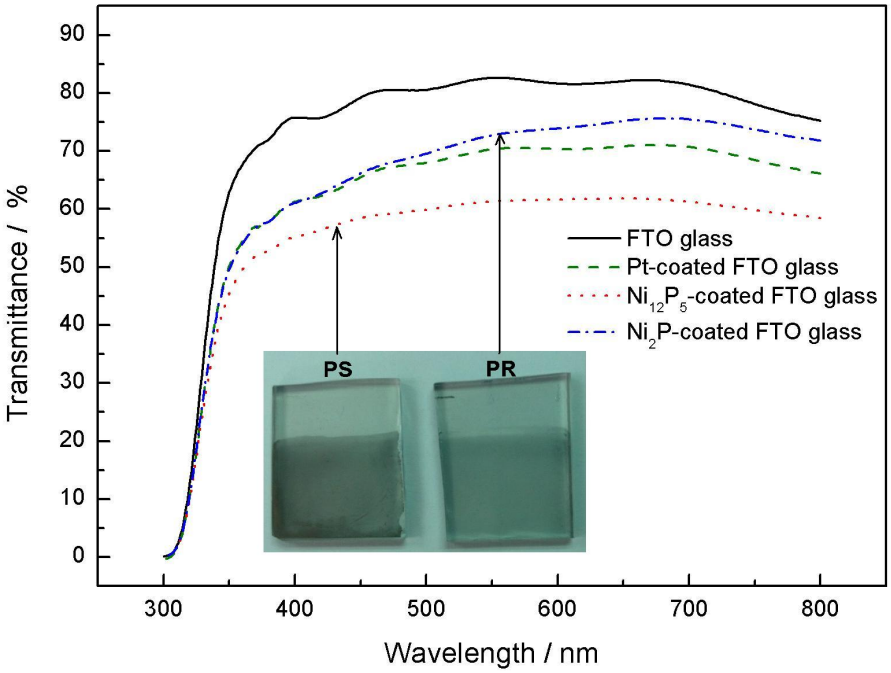

Fig. S4 UV-Vis absorption spectra of bare FTO, Pt-coated FTO, $Ni_{12}P_5$-coated FTO (PS), and Ni_2P-coated FTO (PR) glass electrodes. The inset shows the photographs of $Ni_{12}P_5$ and Ni_2P deposited by PS and PR methods, respectively.

Electrochemical impedance

Fig. S5 shows the Nyquist plots of symmetrical cells with one pair of electrodes consisting of Pt or nickel phosphide. The obtained EIS spectra were fitted with the equivalent circuit as shown in the inset of Fig. S5. The resistance values obtained from the EIS spectra are shown in Table S1. The resistance element R_s in the high-frequency region results from the sheet resistance of the FTO substrate. All cells have similar values of R_s (close to 12 Ω), probably due to the same FTO substrate used. The semicircle in the high-frequency region represents the charge-transfer process at the electrode/electrolyte interface, and another one in the low-frequency region is attributed to the Nernst diffusion impedance (Z_d) process of I^-/I_3^- redox species within pores. The semicircle in high-frequency region is composed of two overlapped semicircles because two electrodes in a cell may not be completely identical. Therefore, the charge-transfer

resistance of cell R_{ct} is the sum of R_1 (electrode 1) and R_2 (electrode 2). It was previously reported that the value of R_{ct} plays an important role in determining the photovoltaic performances of the DSCs. The charge-transfer resistances of cells with Pt, Ni_2P (PR), and $Ni_{12}P_5$ (PS) electrodes are 4.15, 3.44, and 286.24 Ω, respectively. The cell consisting of two $Ni_{12}P_5$ (PS) electrodes possesses a large R_{ct} of 286.24 Ω. After removing the Ni-rich regions in the bulk nickel phosphide alloy, the R_{ct} of cell consisting of two Ni_2P (PR) electrodes can be dramatically reduced to 3.44 Ω, which is even below that of cell consisting of a pair of Pt electrodes (4.15 Ω). This result highlights the superior electrocatalytic activity of Ni_2P electrode prepared by PR deposition over the $Ni_{12}P_5$ electrode prepared by PS deposition. The Nernst diffusion impedances of the cells with Pt, Ni_2P (PR), and $Ni_{12}P_5$ (PS) electrodes are 2.35, 1.75, and 13.81 Ω, respectively. The diffusion of I^-/I_3^- is faster within the thin porous Ni_2P film. As expected, ultrathin Ni_2P film composed of porous nanospheres shows superior electrochemical features, including the lower charge-transfer resistance and Nernst diffusion impedance. The new electrode structure provides more pathways for the electrolyte to percolate into the interior of the nanospheres.

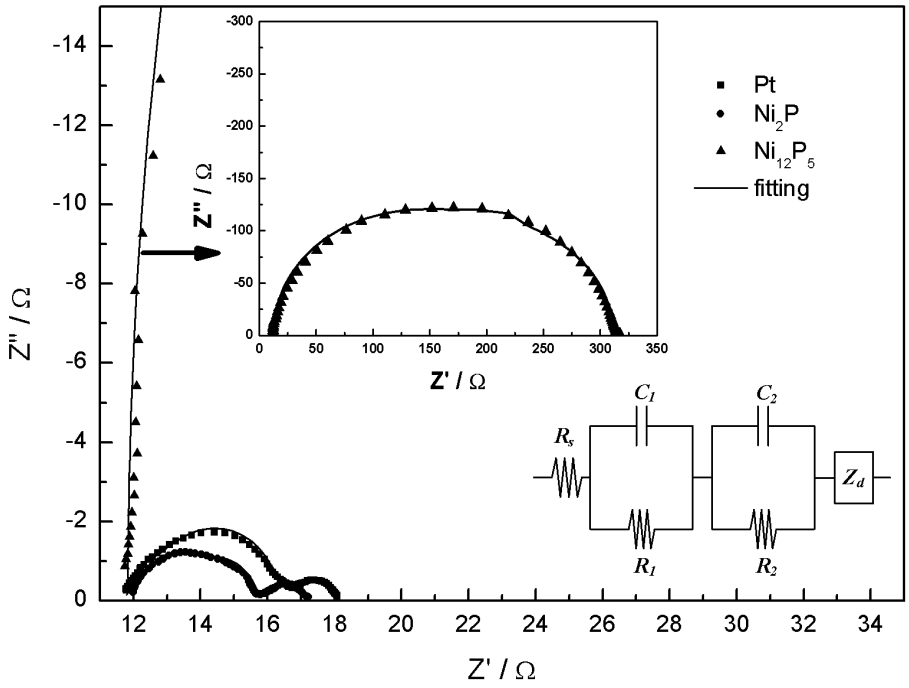

Fig. S5 Nyquist plots of symmetrical cells with one pair of electrodes consisting of Pt, $Ni_{12}P_5$ (PS), or Ni_2P (PR).

Table S1 Resistance values of cells employing the Pt, Ni_2P (PR), and $Ni_{12}P_5$ (PS) electrodes obtained from the electrochemical impedance spectra

Electrode	R_s (Ω)	R_1 (Ω)	R_2 (Ω)	R_{ct} (Ω)	Z_d (Ω)
Pt	11.75	1.15	3.00	4.15	2.35
Ni_2P	12.04	1.95	1.49	3.44	1.75
$Ni_{12}P_5$	11.80	108.51	177.73	286.24	13.81

References

1. S. S. Djokić, *J. Electrochem. Soc.*, 1999, **146**, 1824-1828.
2. H. Sun, D. Qin, S. Huang, X. Guo, D. Li, Y. Luo and Q. Meng, *Energy Environ. Sci*., 2011, 4, 2630-2637.
3. M.-S. Wu, C.-H. Tsai and T.-C. Wei, *Chem. Commun.*, 2011, **47**, 2871-2873.
4. J. Crousier, Z. Hanane and J. P. Crousier, *Thin Solid Films*, 1994, **248**, 51-56.